JOURNAL OF MATERIALS RESEARCH AND TECHNOLOGY 2023;25:4125–4138

Available online at www.sciencedirect.com

jmr&t Journal of Materials Research and Technology

journal homepage: www.elsevier.com/locate/jmrt

The study of screw extrusion-based additive manufacturing of eco-friendly aliphatic polyketone

Danka Labus Zlatanovic [a,b,*], *Jörg Hildebrand* [a], *Jean Pierre Bergmann* [a]

[a] *Department of Production Technology, Technische Universität Ilmenau, 98693 Ilmenau, Germany*

[b] *Department of Production Engineering, Faculty of Technical Science, University of Novi Sad, 21000 Novi Sad, Serbia*

ARTICLE INFO

Article history:
Received 24 March 2023
Accepted 23 June 2023
Available online 26 June 2023

Keywords:
Aliphatic polyketone
Extrusion-based additive manufacturing
3D printing

ABSTRACT

Aliphatic polyketone is a new-age eco-friendly, high-performance engineering thermoplastic. However, its potential for replacing other polymers depends on its ability to be processed. Considering that the first aliphatic polyketone suitable for processing was developed relatively recently (2015), the material gained new research potential. In this paper screw extrusion-based process was developed for additive manufacturing of aliphatic polyketone. A detailed characterisation of the process and printed samples was done. It was shown that the extruder-base process can produce stable additive-manufactured parts depending on printing speed (process parameters). The interpass temperature has a significant influence on printing properties and it depends on printing speed (travel speed of building platform and extruder rotational speed). With the increase in the printing speed, the interpass temperature increases as well. If it is low causes insufficient heat for diffusion to occur causing delamination and if it is too high causes geometrical deviation of workpieces which leads to defects causing a reduction in inter-road strength. The tensile strength of specimens with raster angle 0° was 62.7 ± 1.4 MPa, which is slightly higher than the tensile strength of base material guaranteed by the supplier (60 MPa) while the elongation up to the first crack was 32.8 ± 4.6%. Iinter-road strength in specimens with a raster angle of 90° was 37.2 ± 0.8 MPa which is 62% of the base material while interpass temperature was 189 ± 3.3 °C.

1. Introduction

The petrochemical industry is one of the world's most rapidly growing petroleum industries. In modern society, the demand for petrochemical products such as plastic, pharmaceuticals, fertilisers, and textile products has grown rapidly and now dominates the global chemical market [1]. However, the production of plastic is one of the fast-growing and most significant contributors to global greenhouse-gas emissions. More than 99% of plastic comes from fossil fuel feedstocks, which makes them the fastest-growing form of oil consumption globally. To avoid overshooting the 1.5-degree warming target, total emissions must stay below the remaining 420 to 570 billion tonnes of carbon dioxide. Current projections state that the production of plastic alone could generate 53.5 billion tonnes of carbon dioxide emissions by 2050, which is between 9 and 13% of the total earth's carbon budget [2]. Therefore, there is a rising demand for eco-friendly polymers to reduce

* Corresponding author. Gustav-Kirchhoff-Platz 2, 98693, Ilmenau, Germany.
E-mail address: danka.labus-zlatanovic@tu-ilmenau.de (D. Labus Zlatanovic).

https://doi.org/10.1016/j.jmrt.2023.06.223

their carbon footprint and help the global energy sector reach net zero CO_2 emissions by 2050 [3].

Aliphatic polyketone (PK) is an eco-friendly, high-performance engineering thermoplastic. It was first developed far back in the 1940s. However, it could not be melt-processed due to poor thermal stability. The first commercial PK was introduced by Shell in 1996. Still, even then, PK had problems with process stability. The presence of a number of carbonyl groups within the PK chain raised the possibility of cross-linking. This chemical reactivity could be triggered by a wide variety of constituents, including sizing agents on glass fibers, ingredients in colourants, or interaction with other polymers. Even adding the PK materials into a machine that was not adequately purged could very fast result in cross-linking. This caused limited commercial use of PK. Nevertheless, in 2003 Korean company Hyosung bought all Schell patents and started research independently. The first commercial line of new-age stable aliphatic polyketone for extrusion and injection moulding was introduced in 2015 [4]. This means that new-age aliphatic polyketone is a new generation of PK which started to be commercially processed less than ten years ago.

Compared to other aliphatic polymers such as polyethylene with a melting point around 140 °C [5], polyketone copolymers have significantly higher melting point (between 220 and 255 °C) [6]. This increase of the melting point is a result of strong interactions between the highly polar carbonyl groups of adjacent polymer chains [7]. In contrast to aromatic polyketone, it is made from cheap monomers (copolymer of ethylene and CO or terpolymer of ethylene, propylene, and CO). The carbon monoxide monomer can be converted from CO_2, an industrial byproduct. This way, polyketone could contribute to reducing CO_2 emissions and thus their raw material recycling. Furthermore, the sustainability of PK material benefits from the product lifecycle through the carbon footprint reduction compared to other polymer materials. E.g. PK base resin production emits up to 61% less CO_2 than nylon and polyoxymethylene (POM) [8].

PK combines good chemical and hydrolysis resistance necessary to meet the challenges of severe applications in chemical, fuel contact or high-moisture environments. Moreover, PKs have an excellent balance of engineering properties such as excellent wear and friction properties, tensile and impact properties and super-low permeability (e.g. PK can achieve more than 230% higher impact strength compared to nylon) [9,10]. In addition, a unique feature of injection moulded polyketone is the highest elongation (more than 30%) regardless of humidity compared to any other semi-crystalline polymer. Furthermore, the yield strain is above 20%, which is high compared to polylactide acid (PLA) and acrylonitrile butadiene styrene (ABS), common filaments that have yield strain in the range of 3–4% [11]. As a result, components made of polyketone can be manufactured in the design phase with a high degree of certainty and without undesirable effects. That makes polyketone suitable for use in additive manufacturing. However, in the Scopus database, there is no reported research on the additive manufacturing of aliphatic polyketone. The only two works in this area is from Garcia-Leiner et al. [12] and Tseng et al. [13]. However, they studied extrusion-based additive manufacturing of two types of aromatic polyketone from the polyaryletherketone (PAEK) family, namely polyetheretherketone (PEEK) and polyetherketoneketone (PEKK).

The first aliphatic polyketone suitable for additive manufacturing was developed by company Jabil Inc. (PK5000) in 2022 so the area from additive manufacturing of aliphatic polyketone is completely unexplored [14]. To avoid additional costs and time consumption for developing and producing polyketone filaments, a new concept initially developed for processing granulated materials can be used [15]. Bellini et al. [16] developed a new single-screw system for screw extrusion-based additive manufacturing of granulate-based ceramic to obtain additive manufactured parts. The novel concept was initially called mini extruder deposition (MED). They tested the influence of the granule size, temperature at the entrance and exit, room temperature, size and the design of the nozzle and deposition speed. It was pioneer research in the field of screw extrusion-based additive manufacturing. The concept of screw extrusion-based additive manufacturing of granulate was further used for processing thermoplastic polymers [17]. According to the drawbacks reported by Bellini et al. [16], a new, improved single-screw was developed by Reddy et al. [18]. They adapted the process and called it the extruder deposition process (EDP) for processing acrylonitrile butadiene styrene (ABS). The influence of nozzle temperature, chamber temperature and road gap on bond strength and surface finish was analysed. Results were compared with the commercial fused deposition modelling (FDM) process. They show that the developed EDP eliminates most of the drawbacks of the systems developed by Bellini et al. [16] and produces components with a higher strength than that achieved in commercial fused deposition modelling (FDM) systems. Zhou et al. [19] developed a screw extrusion-based system for additive manufacturing of a mixture of different materials (heat-sensitive polyvinyl alcohol (PVOH) and its additives). Parts were successfully printed with geometry closely matching those of the design specification. Furthermore, Schmidt et al. [20] developed a granulate-based direct extrusion system for processing ABS and PLA. Produced parts reached tensile strength up to 80% from parts obtained with injection moulding for ABS and up to 99% for PLA.

A similar system was also used for the additive manufacturing of composites. Li et al. [21] processed polymer magnet composite pellets consisting of 65 vol% isotropic NdFeB powder and 35 vol% polyamide (Nylon-12). This method significantly simplified the production of near-net-shape bonded magnets and enabled efficient use of rare earth elements, thus enriching the supply of critical materials.

This paper represents the first detailed study of the additive manufacturing of aliphatic poyketone known to the authors. Considering that the EDP process produces parts with good mechanical properties, without developing expensive moulds and without previous filament production, this research aims to modify the EDP process for additive manufacturing of aliphatic polyketone. However, due to the unstable structure of the polyketone at elevated temperatures, the process faces many challenges. Therefore, a customised extruder for processing polyketone was developed and a detailed characterisation with light microscopy, scanning electron microscopy (SEM), mechanical testing,

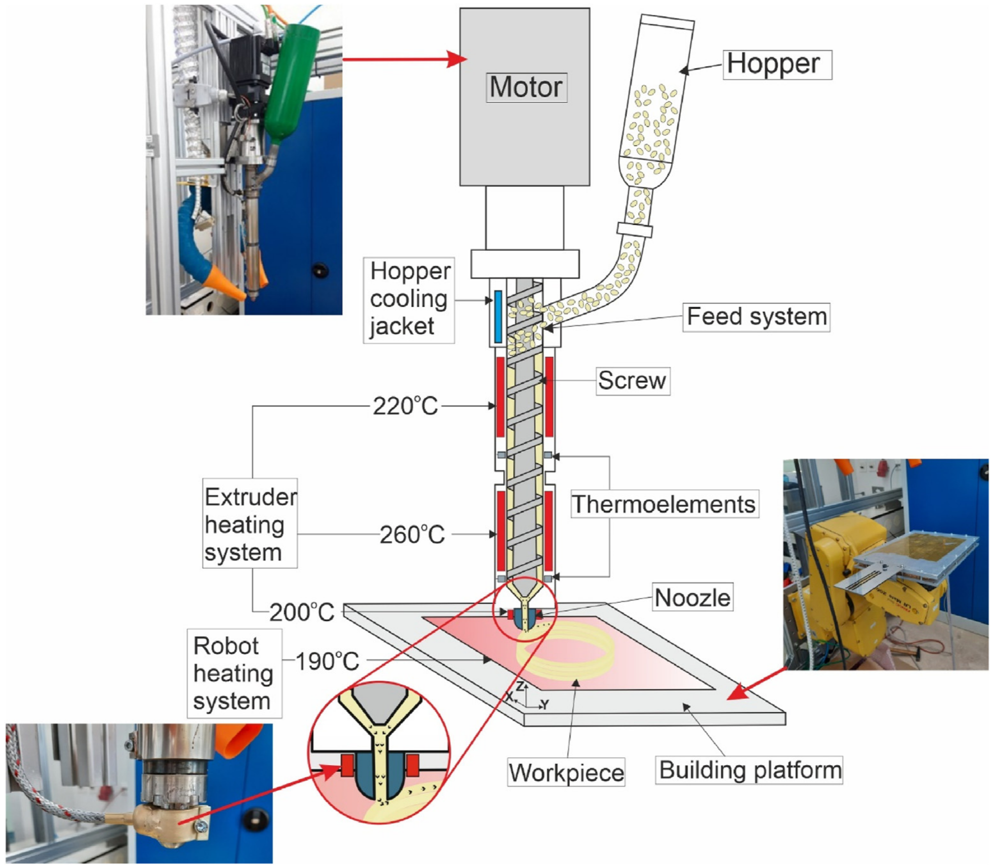

Fig. 1 – Schematic of extruder deposition system (EDS).

differential scanning calorimetry (DSC) analysis and X-ray inspection was carried out. The presented paper highlighted all the challenges during the screw extrusion-based additive manufacturing of aliphatic polyketone and ways to overcome them. The study reveals that polyketone parts can be manufactured successfully with EDP. Therefore, this study represents introductory research in this field and points out the future direction of research.

2. Materials and methods

2.1. *Material*

The granulat used during EDP was made from aliphatic polyketone PK-HM 4773 by supplier AKRO-PLASTIC GmbH [22]. The average granule size is 4.69 ± 0.11 mm. Yield stress, according to the supplier, is 60 MPa. A differential scanning calorimetry instrument (DSC 204 F1 Phoenix) was used to determine the melting point of polyketone ($T_m = 227$ °C) and the glass transition temperature ($T_g = 80.5$ °C). To determine the moisture and melt volume flow rate of polyketone, the INSTRON CEAST MF 20 instrument was used. The measurement was done according to DIN ISO 1133 at temperature 240 °C and at load 2,16 kg. The melt volume flow rate according to supplier was 5.9 × 10 mm^3/10 min.The moisture of polyketone was measured at 105 °C for 20 min. Raw polyketone has 0.2% moisture and after drying for 3 h at 75 °C the moisture was reduced to 0.03%, which is acceptable according to a material supplier.

2.2. *System specifications*

The customised set-up was assembled to adjust the EDP for the processing of polyketone (Fig. 1). The extruder ExOn10 from Herz GmbH, Germany, with printed Fanuc Robot LR Mate 200iB with 6 axes was used. The maximal rotational speed of

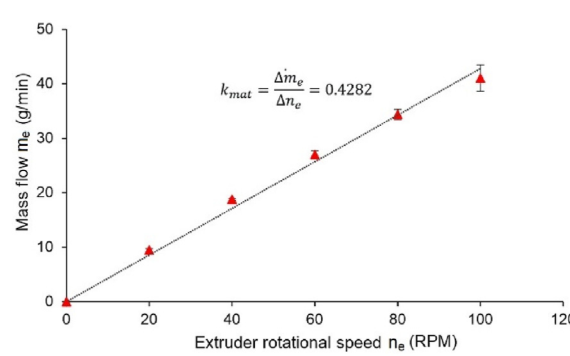

Fig. 2 – Extruder output characteristic for polyketone.

the extruder and motor were 175 RPM and 3500 RPM, respectively. The maximal temperature which can be set is 350 °C with accuracy of ±2 °C. The extruder and the building platform are regulated separately. The building platform (240 × 330 mm) is assembled with a robotic arm and has an embedded heating system with a maximal temperature of 200 °C. During experimental tests, the temperature of the building platform was set to 190 °C. To increase the adhesion between the workpiece and the building platform, the building platform top side was covered with a single-layered polyimide tape.

The main elements of the plasticising unit are a granulated hopper with a feed system, screw and nozzle. Hopper and feed systems are designed to provide a constant feeding velocity. The plasticising unit is exposed to three different temperature zone. In the first zone where the granulate enters the unit, the unit was constantly cooled. In the second zone, the plasticising unit is heated at 220 °C according to the recommendations of the polyketone supplier for injection moulding [22]. In the third zone, the recommendation from the supplier was 250 °C. However, during the preliminary test, it was found that at 250 °C, polyketone does not melt sufficiently. Far better results were achieved at 260 °C. In the area between the third zone and the nozzle exit, the polyketone solidified due to a quick cooling of polyketone in contact with the cold nozzle. Therefore, an additional heating element was placed at the nozzle to provide an unhindered flow of molten material. The temperature was set at 200 °C. All temperatures were set constant during the experimental tests. The nozzle diameter was 4 mm. It was chosen based on preliminary research, which showed that with the presented set-up without additional cooling, a diameter of 4 mm is the largest diameter that can ensure the production of parts with a stable geometry. The system was programmed to create a cylindrical workpiece with a diameter of 120 mm and high of 72 mm. During the process, the temperature was monitored with an infrared camera Optris PI450. Emissivity was set to 0.9. The camera has a temperature range between −20 and 900 °C and an accuracy of ±2 °C. The thermal emissivity was calibrated with thermoelements. The interpass temperatures and line temperatures over the printed workpiece were extracted from thermograms. They have been measured in three different spots and distance of 5 mm between every two strand (for interpass temperatures) and in middle of every strand (for line temperature).

2.3. *Sample characterisation*

After processing the workpieces, a detailed characterisation was done. The materialography was performed with an optical microscope, scanning electron microscope and X-ray inspection. All test samples were finely ground with abrasive paper (grit 360 to 2500) and polished with diamond suspension (6 μm). Colloidal silica of 0.05 μm was used as a final polishing step. The cross-sectional examination was done with a light microscope Zeiss AxioScope.A1. The fracture mode of the samples was examined with a scanning electron microscope (Hitachi S-4800) operating at 15 kV. To detect defects X-ray inspection system Nanomex 180 from company GE Sensing (USA) was used. A maximum acceleration voltage is 180 kV, and a maximum X-ray power is 20 W with a digital detector and sensor GE DXR250RT.

A differential scanning calorimetry instrument Netzsch DSC 204 F1 Phoenix with aluminum sample pans under nitrogen purge (250 ml/min) was used to study the influence of the holding time of polyketone at high temperatures. The sample mass was 1.8 mg nominal, and a new sample was prepared for each run. The samples were heated from 25 to 300° with heating speed 5 K/min.

To analyse the mechanical properties of the additive manufactured workpieces, microhardness and tensile tests were performed. Microhardness tests were done by using the standard Vickers microhardness test with Struers DuraScan 70mashine with 0.1 kg loading. The tests were repeated three times and the standard deviation was calculated. A Hegewald & Peschke Inspect Retrofit universal testing machine with a maximum load of 20 kN was used to test tensile properties. The specimens had prismatic shapes with dimensions (height × width × length) 3 × 20 × 72 mm^2. They were tested in two printing directions with raster angles 0° and 90°. . The tests were repeated three times and results are presented with standard deviation.

3. Parameter optimisation

The process parameters were determined by using the *model of the strand deposition* proposed by Schmidt et al. [20]. The model is based on the assumption of equal mass and volume flow rates inside and outside the extruder considering the same density of polyketone in a solid and molten state. According to the model, the equation for the determination of extruder rotational speed is given in (1):

$$n_e = A_{strand} \cdot V_r \cdot \frac{1}{k_{mat}} \cdot \rho \tag{1}$$

where A_{strand} is the cross-sectional area of the strand, V_r − the travel speed of the building platform, ρ − polyketone density and k_{mat} is a constant that was determined experimentally. For that purpose, the mass output after 120 s as a function of extruder rotational speed was measured. All measurements were repeated three times and results obtained from the test are presented in (Fig. 2).

Expected strand width and height were added in equation (1) to determine the process parameters. According to preliminary experiments, the strand height was set to be in the range of 1.6–4.0 mm (1.6, 2.4, 3.2 and 4 mm). Below 1.6 mm, the cooling rate of the material was too high, which caused the first layer to bend, causing a collision between the nozzle and the first layer during the second layer deposition. A nozzle diameter of 4 mm limits the strand height because a nozzle can extrude a strand with a maximum height of 4 mm. The strand width was set to be 4, 5 and 6 mm. The minimal value of strand width (4 mm) was restricted by nozzle diameter and strand widths above 6 mm caused high geometry deviations. For higher width, a nozzle with a larger diameter should be used.

The travel speed of the building platform was also varied from 10 to 20 mm/s (10, 15 and 20 mm/s). Below the 10 mm/s value, the relative speed between the extruder and the

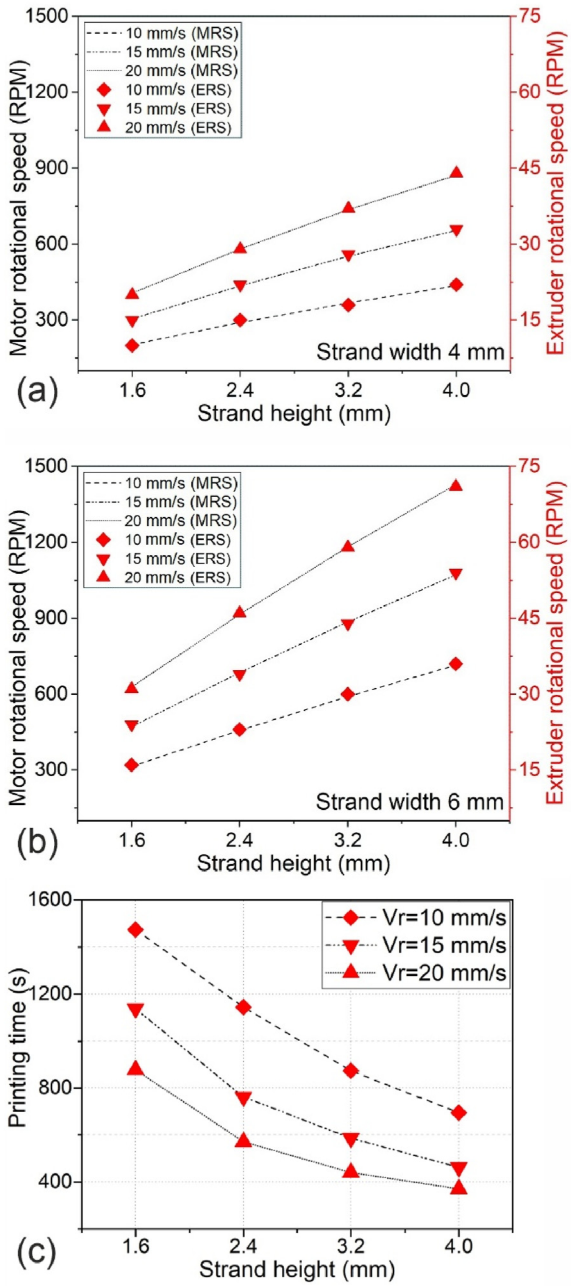

Fig. 3 – Process parameters for: (a) strand width 4 mm; (b) strand width 6 mm and (c) printing time. (MRS – Motor rotational speed, ERS – Extruder rotational speed).

building platform was too low, which caused the lower layer to cool down before the second layer was deposited. That resulted in no bonding between the layers. On the other hand, due to too high relative speed, the workpiece sinks because of the high-temperature accumulation as the layers overlap too quickly. Fig. 3a and b shows the calculated motor and extruder rotational speed according to (1) for two series with different strand widths. In each series, the strand height and speed of the building platform were varied.

Printing time depends on process parameters and programmed workpiece height. The programmed workpiece height was set to be constant for all specimens (72 mm). Fig. 3 cshows that printing time significantly drops with an increase in relative speed, namely, the travel speed of the building platform and extruder rotational speed which increases with the increase of strand height (Fig. 3a and b).

4. Results and discussions

4.1. *Geometrical deviation*

During the extruder deposition process of polyketone, a stabile geometry can be achieved depending on the process conditions. Fig. 4a shows specimens produced with different process parameters. Specimens produced with a strand width of 4 mm provide a more stable geometry than those with a strand width of 6 mm. However, they lose geometrical stability with an increase in the relative speed between the extruder and building platform as well as with the increase of strand volume. That causes the workpiece to sink (sample with strand height 4.0 mm) due to a low-temperature gradient caused by high-temperature accumulation in the high-volume strand. Therefore, lower layers stay softened for a longer time and due to the higher weight of the upper layers, the workpiece begins to sink (loose workpiece height and wall thickness become uneven). The samples with strand height 4.0 mm have also problems with instability because 4.0 mm is also diameter of the nozzle. Therefore, according to the theoretical model two strands should be connected only at one point. Hovewer, in reality the height is decreased because the soft strand is deformed due to gravity and the minimal contact surface between the two strands. In this case, due to unstable contact, we also have an deviation of the strands and there is no proper strand arangment.That can be observed in Fig. 4b, where workpiece height depends on the strand height and travel speed of the building platform. In specimens obtained with a strand height of 4.0 mm and a travel speed of 20 mm/s, the workpiece height dropped by ~20–25% compared to the programmed height in both cases (strand width 4 and 6 mm). Schmidt et al. [20] found that as the strand height increases, the corresponding mass application increases as well. This causes increasing heat storage capacity and consequently slows cooling and hardening, causing dimensional instability.

In some cases, there were slight increases in the height of printed workpieces compared to the programmed height. That is expected during 3D printing with a nozzle due to the Barus effect [23]. The effect occurs because the molecules extend when the melt passes through the nozzle. The highest extension occurs nearby to the wall. After being released from the nozzle, molecules tend to coil up, contract in the flow direction and expand in a direction transverse to the flow. Therefore, extrudate swells because the extruded material expands via elastic recovery at the exit of the nozzle [24].

The second type of geometrical deviation can be observed in samples obtained with a strand width of 6 mm and strand height of 1.6 mm for all three travel speeds of the building platform. This effect occurs due to a too-large contact area between the nozzle and strand. Furthermore, the higher pressure of the nozzle is applied on the strand, which causes

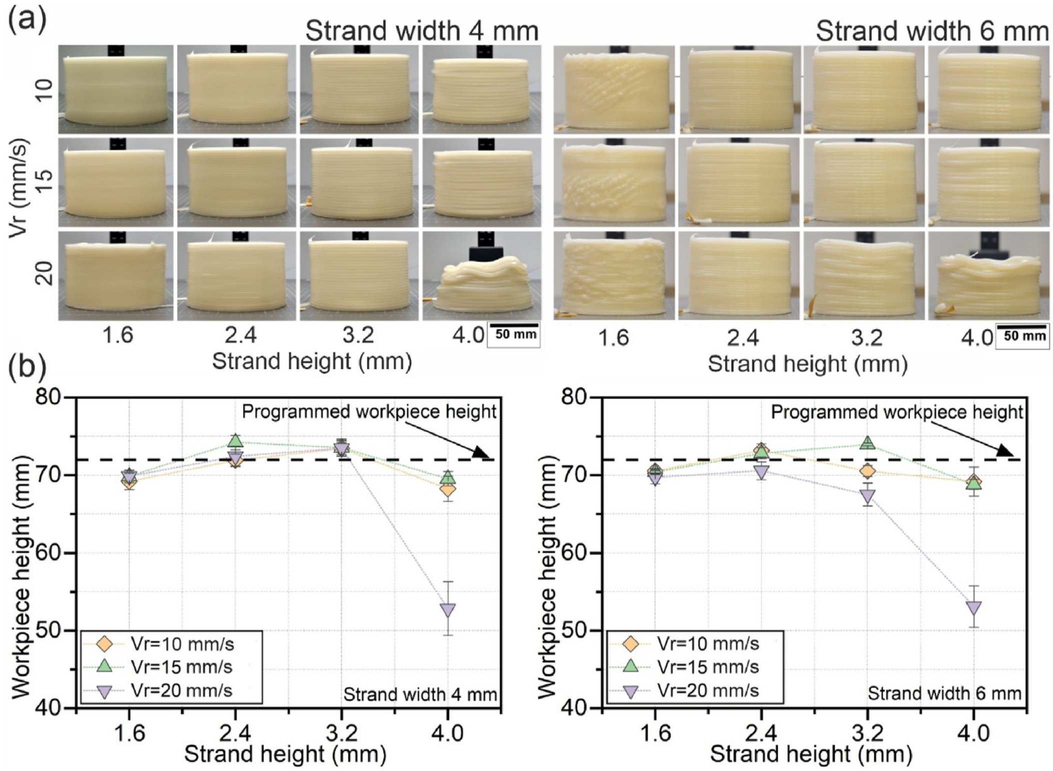

Fig. 4 – (a) 3D polyketone structures obtained with different parameters; (b) workpiece height obtained at different parameters (Vr – travel speed of building platform).

stronger adhesive forces between them. In combination with the low temperature of the substrate layer, as a result of the low relative speed between the extruder and building platform and the faster cooling of the strand, the strand attaches to the nozzle rather than to the substrate layer. As a result, it causes defects, which repeat themselves in the next layers in the form of a wave. Bellini et al. [16], during the deposition of a single-road wall box with mini extruder deposition of ceramics, observed that below minimal temperature, the delivered material does not adhere to the subtract but remains attached to the external surface of the nozzle. Due to the nozzle temperature, this material melts and stitches onto previously deposited roads, damaging the already-built layers.

4.2. *Thermography*

Thermograms of the workpieces were recorded with a thermal camera to understand the influence of the process parameters on temperature distribution during the process and neck growth between the strands Fig. 5. In extrusion-based additive manufacturing processes, inter-road bonding is driven by the thermal energy of the semy molten material. Inter-road coalescence takes place in three stages: (i) surface contacting, (ii) neck growth and (iii) diffusion and randomisation [25].

Presented thermograms (Fig. 5.) were captured during the deposition of the last layer right before the end of the process. Thermograms show strong dependence between temperature distribution and relative speed between the extruder and the building platform. With the increase in the relative speed (travel speed of the building platform and extruder rotational speed), more temperature is accumulated in the workpiece because the bottom layers do not have enough time to cool down before the upper layer is deposited. That causes the heat storage capacity of the workpiece to increase and therefore cooling rate to decrease [20]. Fig. 6a and b shows the example of temperature distribution in specimens with a strand width of 4 mm measured vertically in line at the end of the process for different travel speeds (Fig. 6a) and strand heights (Fig. 6b). It can be observed that in both cases at the beginning and the end of the process, temperature are close. At the beginning of the process, heating of the building platform has a high influence on the first few strands, which is why in all cases temperature decreases after the approximately third strand and afterwards increases again. At the end of the process, the last measurement was done in the top strand directly behind the nozzle where the temperatures are similar. However, a high difference can be observed between those two values. It can be seen that workpieces printed with lower travel speeds and lower strand heights (lower relative speeds) have reduced temperatures. In the workpiece printed with a travel speed of 10 mm/s temperature varies from ~90 to ~205 °C while in the workpiece welded with a travel speed of 20 mm/s from ~125 to ~215 °C. Slightly higher influence has strand height where in a workpiece printed with a strand height of 1.6 mm, temperatures vary from ~96 °C to ~210 °C while in a workpiece printed

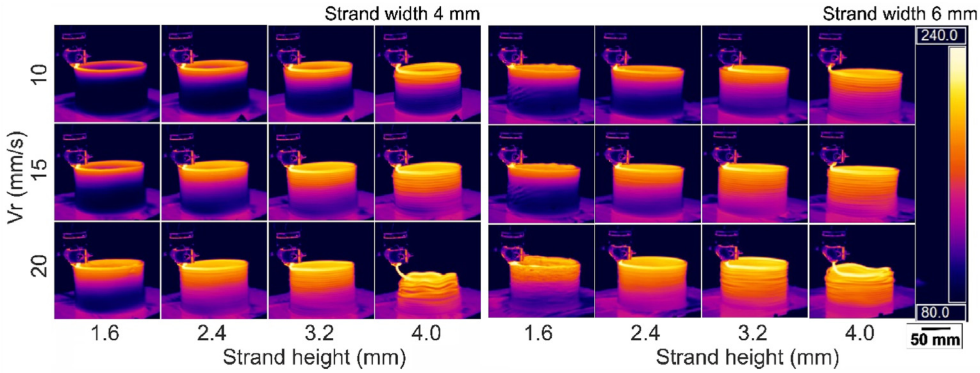

Fig. 5 – Thermograms [°C] of the specimens obtained with different strand widths and heights at different travel speeds of the building platform (Vr).

with 4 mm strand height temperatures vary from ~135 °C to ~205 °C. This effect causes workpieces printed with high relative speeds to have a stronger adhesion but also after some point they lose their geometry.

Furthermore, the printing time of the workpiece is shorter with an increase in relative speed. That confirms the assumption that the bottom layers remain softened before the upper layers are deposited, causing the sinking of the geometry under pressure. It is additionally pronounced in workpieces with the maximum strand cross-section (4.0 × 4.0 mm) due to the increased weight of the strand. The lowest temperatures are captured in specimens with a strand height of 1.6 mm and strand width of 4 mm where delamination can occur due to low temperature. The highest temperatures can be found in specimens with the highest travel speed of the building platform and highest strand

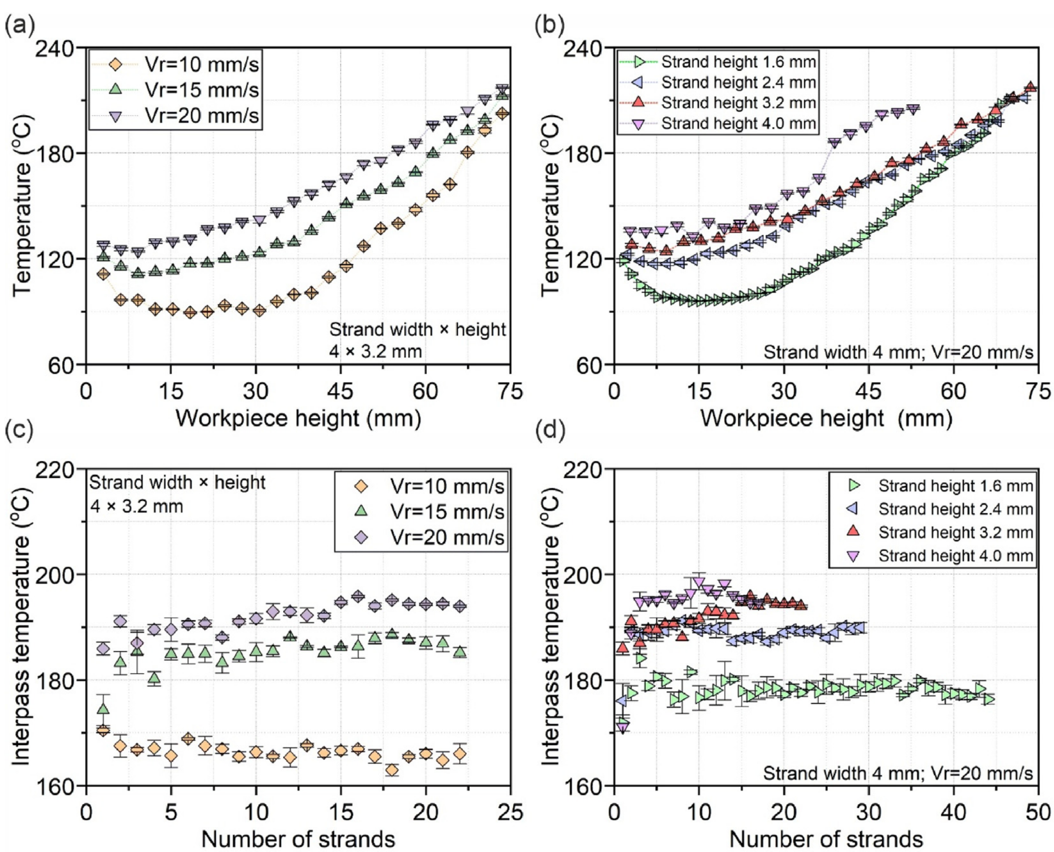

Fig. 6 – Results of temperature measurements: (a) interpass temperature for different travel speeds; (b) interpass temperature for different strand heights (c) temperatures measured in strands over the workpiece height for different travel speeds; (d) temperatures measured in strands over the workpiece hight for different strand heights.

heights where the sinking of the workpiece is evident. To obtain samples with good mechanical properties and stable geometry, a compromise has to be found. This will be discussed in chapter 3.4, together with inter-road bond strength.

The relative speed of the printing process also influences interpass temperature Fig. 6c and d. With the increase in the travel speed of the building platform, the interpass temperature increases as well. The average interpass temperature in a workpiece printed with a travel speed of 10 mm/s is 166 ± 1.8 °C while in a workpiece printed with 20 mm/s is 192 ± 2.7 °C. Increasing the strand height and thus the rotational speed of the extruder has a similar effect. The workpiece printed with a strand height of 1.6 mm has an average interpass temperature of 178 ± 2.2 °C while the workpiece printed with a strand height of 4 mm has 193 ± 6 °C. The higher deviation is a consequence of geometry deviation which has caused uneven interpass temperature.

4.3. Materialography

Fig. 7 shows cross-section macrographs of the workpiece wall obtained with a travel speed of building platform of 15 mm/s and strand width of 4 mm. The macrographs were taken in the middle of the specimen at a length of 16 mm. Macrographs show that specimens have no visible defects, (except pores in specimens obtained with a strand height 4 mm pointed with a black arrow) and there are no visible bonding lines. It can be assumed that fusion between the strands occurred. However, a notable difference in the shape of the strand is to be seen. With the increase of the strand height, the waviness of the specimen surface (red arrow) increases and the inter-road bond line (blue arrow) decreases up to 50%. This can significantly decrease the loadability of the component and increase the need for postprocessing. Reddy et al. [18] proved that there is a direct correlation between road gap and inter-road bond strength. They contributed to the decrease in the contact area between the roads as the road gap increased. Moreover, if the specimen needs to be post-machined, this reduces the effective wall thickness. Therefore to obtain better mechanical properties and effective wall thickness it is necessary to set lower strand heights. However, that increases the processing time and directly affects productivity.

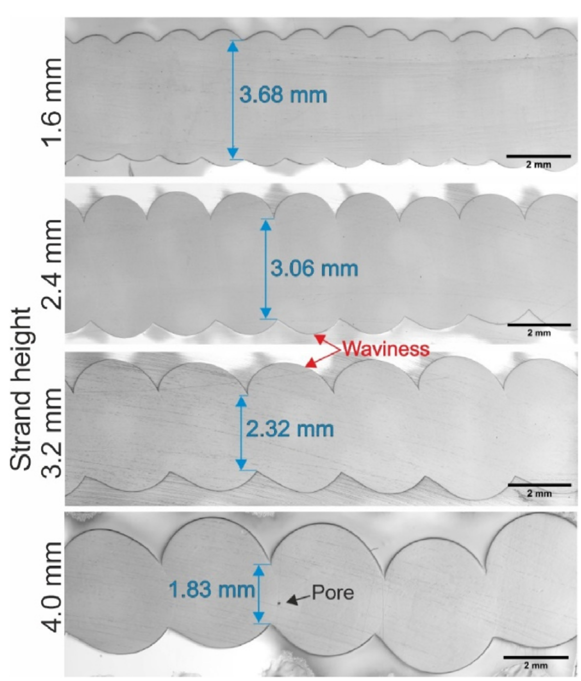

Fig. 7 – Macrographs of the specimens obtained with a travel speed of the building platform 15 mm/s, strand width 4 mm, and different heights. Figures are taken in the middle of the specimen with a 16 mm length.

After a detailed analysis of all specimens in some of them, defects such as pore at the bonding interface (P), delamination (D) and deformed strands (DS) were observed (Fig. 8.). Table 1 shows the influence of the process parameters such as travel speed of the building platform and strand widths and heights on defect occurrence. It can be seen that the most appearing defects are pores and deformed strands. Most affected are specimens obtained with strand width × height 6.0 × 1.6 mm. Considering that pores at the bonding interface are mostly in combination with deformed strands, it can be assumed that due to irregular deposition of the strands, the air stays entrapped between layers causing pores to occur. Visible traces of delamination were found in samples printed with a travel speed of 10 mm/s, strand width of 4.0 mm and heights of 1.6 and 4.0 mm. In the specimen obtained with a 1.6 mm strand height, the delamination occurred due to the low interpass temperature, which confirms the assumption from chapter 3.2. Bellini et al. [16] also found that there is a temperature limit value below which the strength of the interface between two adjacent roads is not sufficient to ensure satisfactory bonding conditions. In the case of the specimen with a strand height of 4 mm, deviation from geometry occurred due to a combination of the high accumulated temperature in the workpiece (Fig. 6) combined with a high volume of strands.

An X-ray inspection was done to ensure that the specimen without defect did not have defects in another region than those tested in cross-section on macro images. Fig. 9 shows X ray images from two specimens without defects. In both figures, the upper part of the workpiece from the top side can be seen. No visible defects can be found. Brighter areas represent the bonding line where the cross-section of the wall is thinner compared to the rest of the part. However, no visible pores or delamination can be seen.

4.4. Mechanical properties

To understand the influence of process parameters on the quality of the printed workpieces mechanical properties were tested. According to hardness tests, no difference was found in the specimens obtained with different parameters. Likewise, hardness was the same for printed samples and granulate and it was 10.2 ± 0.13 HV. Similar results were obtained with the tensile strength of all specimens when the tests were done in the direction of printing with a raster angle 0° (62.7 ± 1.4 MPa). This value is slightly above the value given by the material supplier for granulate (60 MPa). The elongation up to the first crack was 32.8 ± 4.6% which was significantly lower compared to those of granulate (>300%). This can be attributed to the change in crystallinity after remelting, which will be explained in chapter 3.6. However, the inter-road bond

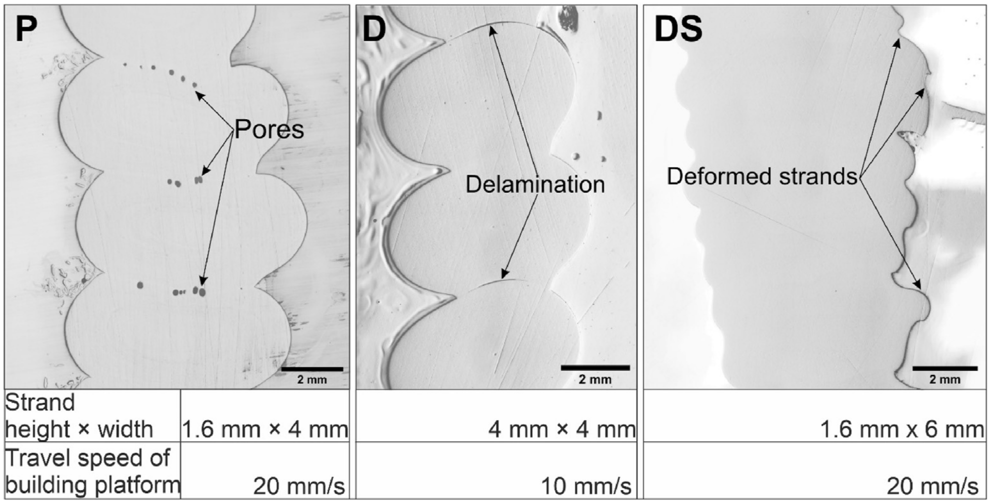

Fig. 8 – Possible defects found in the cross-section of the specimen wall (P-Pores, D-delamination and DS-deformed strands).

strength of specimens obtained in a direction normal to the printing direction depends significantly on process parameters and interpass temperature (Fig. 10). Considering the travel speed of the building platform, the trend is the same in all specimens. All specimens with the same strand height show increase in strength with an increase in travel speed. This can be attributed to the fact that with an increase in the relative speed between the extruder and the building platform the higher interpass temperature is obtained and therefore a better remelting of the layers between occurs. Reddy et al. [18] have found during direct extrusion of ABS that, inter-road strength increases by 9.5% with the increase of nozzle temperature by 13%. They claim that bond strength increases with the increase of the temperature due to better adhesion between the roads up to some point. However, if the temperature is too high, the degradation of the polymer occurs and bond strength starts to decrease.

The highest bond strength 37.2 ± 0.8 MPa was obtained in the specimen printed with strand width × height 6.0 × 2.4 mm and Vr = 20 mm/s followed by a sample with strand width × height 6.0 × 3.2 mm with the same travel speed of building platform. That is 60–62% strength of the base material and 57–59% of the strength obtained in specimens tested in the printing direction, similar to results obtained by Tseng et al. [13]. During line printing of Polyether ether ketone (PEEK) with screw-extrusion-based additive manufacturing ~64% of bulk material strength was achieved, which is slightly higher compared to PK specimens.

Specimens printed with a strand width of 4 mm lose their strength with increased strand height. This can be attributed to the fact that during the printing of specimens with lower strand height a higher pressure on the strand was applied. However, workpieces with strand width of 6 mm show an irregular trend. It seems that defects have a high effect on mechanical properties. Specimens built with a strand height of 1.6 mm have the lowest strength. This can be attributed to the fact that those specimens have low interpass temperatures combined with pores at the bonding line and deformed strands. In the literature on additive manufacturing, the effect of printing layer thickness on mechanical properties is controversial. Some researchers claim that the higher the thickness, the better the mechanical properties are, and others do the opposite [26,27]. This research shows that the best results lie somewhere in between.

The diagram of tensile force vs position for specimens built with a travel speed of 15 mm/s and strand width of 6 mm is presented in Fig. 11. It can be seen that the specimen tested with raster angle 0° has a different tensile elastic modulus compared to specimens with raster angle 90°. Furthermore, a high difference in elongation can be observed as well. This implies that printed polyketone is a highly mechanical anisotropic material which is commonly for 3D printed parts

Table 1 – Defects found in specimens with different process parameters.

Travel speed of building platform (mm/s)	Strand width							
	4 mm				6 mm			
	Strand height (mm)				Strand height (mm)			
	1.6	2.4	3.2	4.0	1.6	2.4	3.2	4.0
10	D			P; D	P; DS			
15				P	P; DS			P
20	P; DS			P; DS	P; DS		DS	P; DS

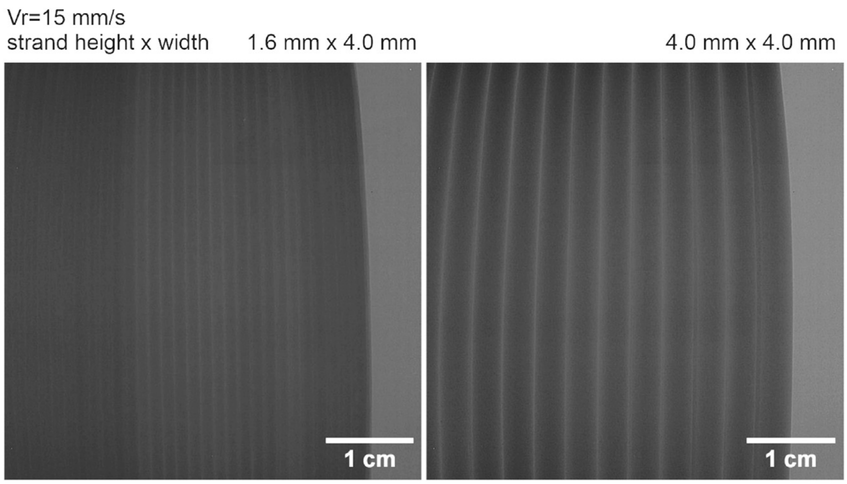

Fig. 9 – X-ray inspection results of workpieces obtained with strand width 4 mm and height 1.6 and 4.0 mm as shown in the figure. Travel speed was 15 mm/s.

[27]. Contributing factors in mechanical anisotropy are air gaps/voids, build orientation, layer delamination and raster angle. Week interlayer bonding can also be the result of the low molecular diffusion and low cross-linking between the polymer layers during deposition. Furthermore, anisotropy is mostly affected by the polymer molecules aligning themselves with the direction of printing after extrusion through the nozzle. In specimens with a raster angle 0° the molecules tend to align in direction of the stress axis, making it the strongest direction. Likewise, weak interlayer bonding can lead to layer delamination [28]. Anisotropy was found in most additive manufactured parts obtained with different techniques such as selective laser sintering (SLS) [29], fused deposition modelling (FDM) [26] etc.

4.5. *Fractured surface*

Fig. 12 shows a fractured surface of two specimens printed with a travel speed of 20 mm/s and strand width of 4.0 mm. The fracture surface shows that the fracture was brittle because the surface has a river pattern which is a typical characteristic of brittle fracture [30]. The difference between the two specimens is in the strand height (1.6 mm and 4.0 mm). In both cases, the strand width is 4.0 mm. At the inter-road surface, pores can be observed, which can significantly reduce inter-road bond strength [31]. Furthermore, inter-road delamination with a combination of brittle failure through the strand can be observed in both specimens. The difference is that in the specimen with a strand height of 1.6 mm the brittle fracture through the strand prevails and in the specimen with a strand height of 4.0 mm, delamination prevails. This can also be correlated to inter-strand bond strength. The specimen with a strand height of 1.6 mm has higher strength (33.2 ± 4.9 MPa) compared to the specimen with a strand height of 4.0 mm (24.3 ± 6.6 MPa). In the specimen printed with 1.6 mm the delamination of layers in strands rather than between strands can be observed, indicating that the inter-strand bond was higher than the intermolecular bond in the strand.

4.6. *DSC Analysis*

Fig. 13 shows dynamic scanning calorimetry (DSC) thermographs of polyketone granulate (a) and two specimens in the

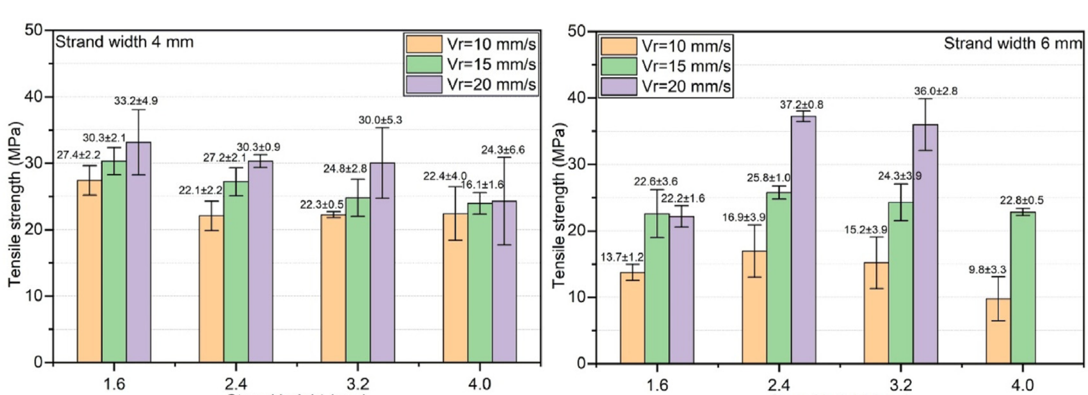

Fig. 10 – Inter-road bond strength.

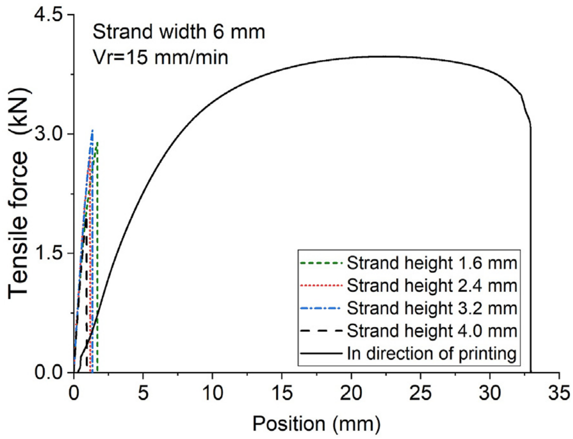

Fig. 11 – Tensile force vs position curves for different strand heights compared to the specimen obtained in the printing direction.

middle, printed with the same travel speed of the building platform (20 mm/s) but with different strand cross-sections (b) 1.6 × 4.0 mm and (c) 4.0 × 4.0 mm. Those two samples were chosen because they have significantly different interpass temperatures (178 ± 2.2 °C and 193 ± 6 °C respectively). The degree of crystallinity (X_c) for the PKs was calculated using the equation $X_c = \Delta H_m/\Delta H_m^0 \times 100\%$, with DSC data where ΔH_m and ΔH_m^0 refer to the heat fusions of the used sample and 100% crystalline PK (227 J g^{-1}), respectively [32]. Granulat was exposed to only one thermal cycle during granulat production while extruded parts underwent two thermal cycles during granulat production and extrusion, which according to Holt et al. [33] has a strong influence on material properties.

Results show a clear difference between granulate and printed parts. Granulate has a higher melting temperature, but lower heat of fusion and crystallinity compared to both printed parts. The decrease in melting temperature from 226.5 °C to 221.6 °C and 222.6 °C, respectively, is caused by the second thermal cycles to which specimens were exposed during extrusion. Holt et al. [33] have observed a decrease in melting temperature with every melting–cooling cycle. They found the same trend in all three different aliphatic polyketones tested. The observed melting behaviour is likely due to condensation reactions that arise in the melt-holding range. These reactions cause cross-linking of the polymer chains.

However, the heat of fusion and crystallinity are higher in printed samples 88.78 J/g and 39.11% for the specimen (1.6 × 4.0 mm) and 91.94 J/g and 40.50% for the specimen (4.0 × 4.0 mm) compared to granulate 75.22 J/g, and 33.14%, which is opposite to result obtained in Ref. [33]. This can be attributed to the fact that printed parts were cooled on air and granulate in production was cooled in water, according to the material supplier. Therefore cooling rates of granulate were higher. So basically, with slow cooling, there is more time for crystallisation. This can also be supported by the fact that crystallinity is slightly higher (1.39%) in the sample with higher interpass temperature (4.0 × 4.0 mm) compared to (1.6 × 4.0 mm). Furthermore, the specimen (4.0 × 4.0 mm) has a higher strand volume causing an increase in heat storage capacity which leads to a decrease in cooling rate compared to the specimen (1.6 × 4.0 mm). This is supported by research from Hu et el. [34], who have investigated the influence of the cooling rate of semi-crystalline polypropylene and found that crystallinity decreases as the cooling rate increases. Even though tensile strength is higher in specimens 1.6 × 4.0 mm (33.2 ± 4.9 MPa) than in specimens 4.0 × 4.0 mm (24.6 ± 6.6 MPa), this cannot be explained by crystallinity because the higher influence on strength tested with raster angle 90 °C have bonding line conditions (pores, adhesion, etc.) However, considering tensile properties in specimens tested with a raster angle 0 °C some correlation can be driven, especially considering ductility.

According to Hocker et al. [35] crystallinity has a high influence on ductility. They have found that the ductility of semi-crystalline polyamide decreases with an increase in crystallinity. The same behaviour is found in printed specimens where elongation decreased significantly compared to the granulate. The elongation was 32.8 ± 4.6% measured in specimens with raster angle 0°, which was significantly lower compared to those of granulate (>300%). However, there is no significant influence on tensile strength. The strength of specimens tested with raster angle 0° was 62.7 ± 1.4 MPa,

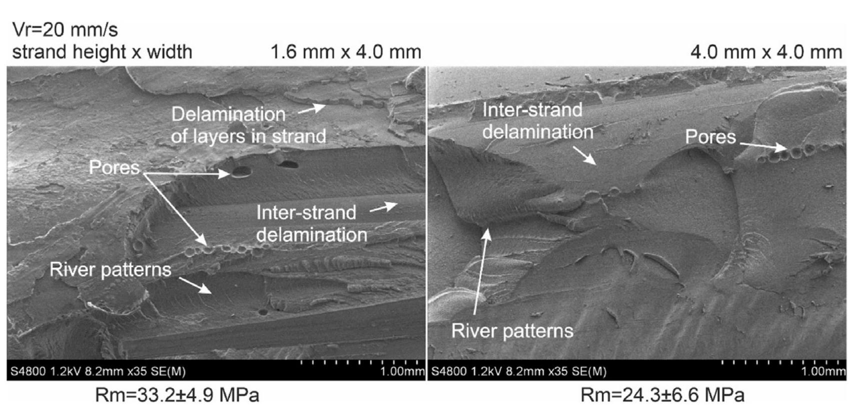

Fig. 12 – Fracture surface of specimens printed with a travel speed of building platform of 20 mm/s, strand width of 4 mm and strand height of 1.6 and 4.0 mm.

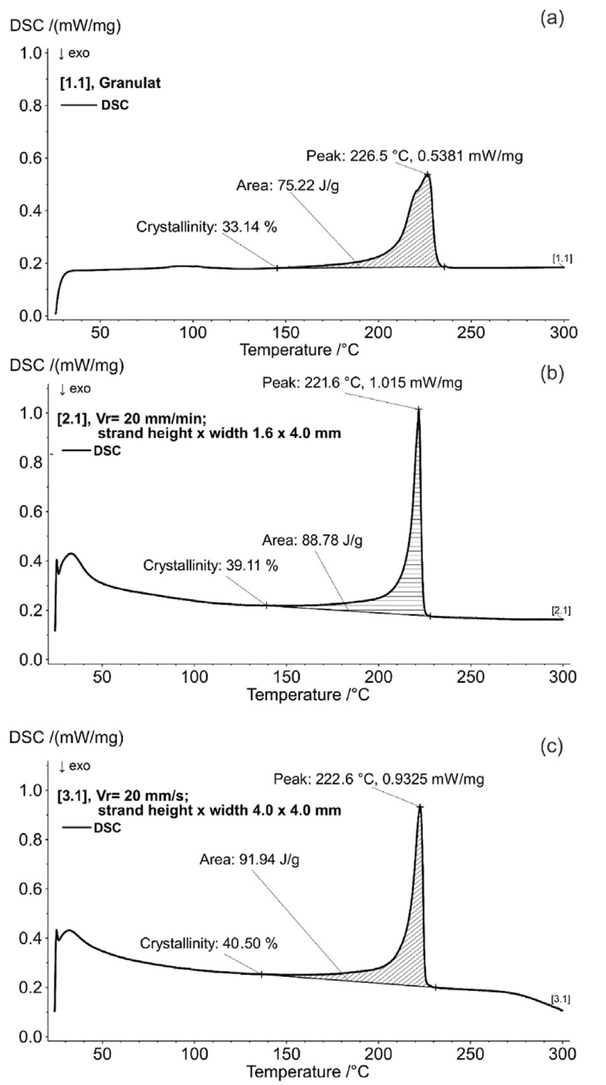

Fig. 13 – Differential scanning calorimetry thermograms of (a) granulate; two specimens printed with a travel speed of the building platform 20 mm/s with (b) strand cross-section 1.6 × 4.0 mm and (c) strand cross-section 4.0 × 4.0 mm.

which is even slightly higher than the tensile strength of granulate guaranteed by the supplier (60 MPa) [22].

5. Conclusions

This paper shows that screw extrusion-based additive manufacturing of aliphatic polyketone can provide reliable printed parts. Furthermore, it reveals new insights into the complex 3D printing process of polyketone. The following broad conclusions were summarised based on the results.

- To obtain printed parts with stable geometry and mechanical properties, a number of influencing parameters have to be taken into account, such as strand cross-section, the rotational speed of the extruder, the travel speed of the building platform and nozzle diameter. Results show that the relative speed of the extruder and building platform has the most significant impact on temperature distribution in the workpiece and interpass temperature, therefore, on workpiece quality as well.
- With the increase of the relative speed, the temperature accumulation in the workpiece increases, which causes an increase in bonding strength but, after some point, significantly affects workpiece geometry. Workpiece starts to sink and layers are no longer stable on one another. Therefore, the printed part is deformed with significantly lower height than the programmed.
- Even though the hardness and tensile strength of the printed specimens with raster angle 0° were not affected by the process, the ductility and inter-road bond strength in specimens with raster angle 90° were affected significantly. The highest inter-road bond strength (62% of granulate strength) was found in the specimen printed with a travel speed of the building platform of 20 mm/s, and a strand cross-section of 2.4 × 6.0 mm where interpass temperature was 189 ± 3.3 °C. Interpass temperature had a significant influence on inter-road strength. If it is low causes insufficient heat for diffusion to occur and if it is too high causes geometrical deviation which leads to defects causing a reduction in inter-road strength.
- A significant drop in ductility (~10 ×) in all specimens, compared to the granulate, is due to a second thermal cycle to which specimens were exposed during extrusion. Process conditions also had an impact on crystallinity. With higher relative speed, the crystallinity was increased as well.

Declaration of competing interest

The authors declare the following financial interests/personal relationships which may be considered as potential competing interests: Jean Pierre Bergmann reports financial support was provided by Bundesministerium für Wirtschaft und Klimaschutz under the program Zentrales Innovationsprogramm Mittelstand (ZF4075144TS9).

Acknowledgement

For financial support, the authors are grateful to Bundesministerium für Wirtschaft und Klimaschutz under the program “Zentrales Innovationsprogramm Mittelstand” (ZF4075144TS9). We acknowledge support for the publication costs by the Open Access Publication Fund of the Technische Universität Ilmenau. Furthermore, the authors would like to express gratitude to Michael Rieck and company AKRO-PLASTIC GmbH for providing us with material and advice for the proper use of PK. We would also like to thank our project partners Martin Bogar from the company Buss mould technology GmbH & Co. KG and Dr. rer. nat. Florian Klimenta from company Ematik GmbH for their support and guidance during the experimental process.

Furthermore, we also want to thank Michel Schlosser from Plastics Technology Group, TU Ilmenau for help with DSC analysis, Maximilian Rohe from Department of manufacturing technology, TU Ilmenau for help with X-ray inspection and Robert Eichler from Department of manufacturing technology, TU Ilmenau for help with specimen production and preparation.

REFERENCES

[1] Alsabri A, Tahir F, Al-Ghamdi SG. Life-cycle assessment of polypropylene production in the gulf cooperation council (Gcc) region. Polymers 2021;13. https://doi.org/10.3390/polym13213793.

[2] Feit S, Muffett C. Climate change: not green, but greenhouse. 2019. https://www.boell.de/en/2019/11/04/climate-change-not-green-greenhouse. [Accessed 12 September 2022].

[3] International Energy Agency. Net zero by 2050. A Roadmap for the Global Energy Sector 2021:224.

[4] Sepe M. Tracing the history of polymeric materials: aliphatic polyketone. 2022. https://www.ptonline.com/articles/tracing-the-history-of-polymeric-materials-part-19. [Accessed 1 March 2023].

[5] Mohammadi H, Vincent M, Marand H. Investigating the equilibrium melting temperature of linear polyethylene using the non-linear Hoffman-Weeks approach. Polymer 2018;146:344–60. https://doi.org/10.1016/j.polymer.2018.05.049.

[6] Hou J, Park C, Jang W, Byun H. Facile fabrication and characterization of aliphatic polyketone (PK) micro/nano fiber membranes via electrospinning and a post treatment process. RSC Adv 2020;11:678–83. https://doi.org/10.1039/d0ra08119a.

[7] Lin H, Pearson A, Kazemi Y, Kakroodi A, Hammami A, Heydrich M, et al. Influence of hygrothermal conditioning on the chemical structure and thermal mechanical properties of aliphatic polyketone. Polym Degrad Stabil 2020;179. https://doi.org/10.1016/j.polymdegradstab.2020.109260.

[8] Polyketone-Based Compounds to Compete with Nylons 6. 66 and POM, https://www.ptonline.com/products/polyketone-based-compounds-to-compete-with-nylons-6-66-and-pom. [Accessed 12 September 2022].

[9] Yang Y, Li S-Y, Bao R-Y, Liu Z-Y, Yang M-B, Tan C-B, et al. Progress in polyketone materials: blends and composites. 2018. https://doi.org/10.1002/pi.5624.

[10] Vavasori A, Ronchin L. Polyketones: synthesis and applications. Encycl. Polym. Sci. Technol.; 2017. p. 1–41. https://doi.org/10.1002/0471440264.pst273.pub2.

[11] Akrotek® Pk – The polyketone with universal qualifications. https://www.distrupol.com/AKROTEK-PK.pdf.chrome-extension//efaidnbmnnnibpcajpcglclefindmkaj/ [Accessed September 27, 2022].

[12] Garcia-leiner M, Streifel B, Macdonald DW, Kurtz SM. Characterization of polyaryletherketone (PAEK) fi laments and printed parts produced by extrusion-based additive manufacturing. Polym Int 2021:1–9. https://doi.org/10.1002/pi.6231.

[13] Tseng JW, Liu CY, Yen YK, Belkner J, Bremicker T, Liu BH, et al. Screw extrusion-based additive manufacturing of PEEK. Mater Des 2018;140:209–21. https://doi.org/10.1016/j.matdes.2017.11.032.

[14] Polyketone-based material for additive manufacturing delivers strength. Chemical Resistance 2022. https://www.plasticstoday.com/medical/polyketone-based-material-additive-manufacturing-delivers-strength-chemical-resistance. [Accessed 15 September 2022].

[15] Valkenaers H, Vogeler F, Ferraris E, Voet A, Kruth J-P. A novel approach to additive manufacturing: screw extrusion 3D-printing. Proc. 10th Int. Conf. Multi-Material Micro Manuf. 2013:235–8. https://doi.org/10.3850/978-981-07-7247-5-359.

[16] Bellini A, Shor L, Guceri SI. New developments in fused deposition modeling of ceramics. Rapid Prototyp J 2005;11:214–20. https://doi.org/10.1108/13552540510612901.

[17] Altıparmak SC, Yardley VA, Shi Z, Lin J. Extrusion-based additive manufacturing technologies: state of the art and future perspectives. J Manuf Process 2022;83:607–36. https://doi.org/10.1016/j.jmapro.2022.09.032.

[18] Reddy BV, Reddy NV, Ghosh A. Fused deposition modelling using direct extrusion. Virtual Phys Prototyp 2007;2:51–60. https://doi.org/10.1080/17452750701336486.

[19] Zhou Z, Salaoru I, Morris P, Gibbons GJ. Development of a direct feed fused deposition modelling technology for multi-material manufacturing. AIP Conf Proc 2016;1769. https://doi.org/10.1063/1.4963614.

[20] Schmidt L, Schricker K, Bergmann JP, Hussenöder F, Eiber M. Characterization of a granulate-based strand deposition process in the FLM-method for definition of material-dependent process strategies. Rapid Prototyp J 2019;25:104–16. https://doi.org/10.1108/RPJ-09-2017-0186.

[21] Li L, Tirado A, Nlebedim IC, Rios O, Post B, Kunc V, et al. Big area additive manufacturing of high performance bonded NdFeB magnets. Sci Rep 2016;6:1–7. https://doi.org/10.1038/srep36212.

[22] Akrotek® Pk-Hm natur (4773) n.d. https://akro-plastic.com/de/produktfilter/details/4773/ (accessed December 6, 2022).

[23] Malkin AY, Goncharenko VV, Malinovskii VV. Barus effect in polymer flows through cylindrical and flat dies. Polym Mech 1976;12:439–44. https://doi.org/10.1007/BF00857716.

[24] Uematsu H, Horisawa N, Horikida T, Tanoue S, Iemoto Y. Effect of carbon fiber on the capillary extrusion behaviors of high-density polyethylene. Polym J 2013;45:449–56. https://doi.org/10.1038/pj.2012.167.

[25] Huang B, Singamneni S. Raster angle mechanics in fused deposition modelling. J Compos Mater 2015;49:363–83. https://doi.org/10.1177/0021998313519153.

[26] Rybachuk M, Alice Mauger C, Fiedler T, Öchsner A. Anisotropic mechanical properties of fused deposition modeled parts fabricated by using acrylonitrile butadiene styrene polymer. J Polym Eng 2017;37:699–706. https://doi.org/10.1515/polyeng-2016-0263.

[27] Zohdi N, Yang RC. Material anisotropy in additively manufactured polymers and polymer composites: a review. Polymers 2021;13. https://doi.org/10.3390/polym13193368.

[28] Es-Said OS, Foyos J, Noorani R, Mendelson M, Marloth R, Pregger BA. Effect of layer orientation on mechanical properties of rapid prototyped samples. Mater Manuf Process 2000;15:107–22. https://doi.org/10.1080/10426910008912976.

[29] Beitz S, Uerlich R, Bokelmann T, Diener A, Vietor T, Kwade A. Influence of powder deposition on powder bed and specimen properties. Materials 2019;12. https://doi.org/10.3390/ma12020297.

[30] Kopp JB, Girardot J. Dynamic fracture in a semicrystalline biobased polymer: an analysis of the fracture surface. Int J Fract 2020;226:121–32. https://doi.org/10.1007/s10704-020-00482-y.

[31] Al-Maharma AY, Patil SP, Markert B. Effects of porosity on the mechanical properties of additively manufactured components: a critical review. Mater Res Express 2020;7. https://doi.org/10.1088/2053-1591/abcc5d.

[32] Cho S, Lee JS, Jang H, Park S, An JH, Jang J. Comparative studies on crystallinity, thermal and mechanical properties of polyketone grown on plasma treated cvd graphene.

Polymers 2021;13:1–15. https://doi.org/10.3390/polym13060919.
[33] Holt GA, Spruiell JE. Melting and crystallization behavior of aliphatic polyketones. J Appl Polym Sci 2002;83:2124–42. https://doi.org/10.1002/app.10165.
[34] Hu Y, Liao Y, Zheng Y, Ikeda K, Okabe R, Wu R, et al. Influence of cooling rate on crystallization behavior of semi-crystalline polypropylene: experiments and mathematical modeling. Polymers 2022;14. https://doi.org/10.3390/polym14173646.
[35] Hocker SJA, Kim WT, Schniepp HC, Kranbuehl DE. Polymer crystallinity and the ductile to brittle transition. Polymer 2018;158:72–6. https://doi.org/10.1016/j.polymer.2018.10.031.